A vortex-based subgrid stress model for large-eddy simulation

Ashish Misra and D. I. Pullin
Graduate Aeronautical Laboratories 205-45, California Institute of Technology, Pasadena, California 91125

(Received 24 September 1996; accepted 16 April 1997)

A class of subgrid stress (SGS) models for large-eddy simulation (LES) is presented based on the idea of structure-based Reynolds-stress closure. The subgrid structure of the turbulence is assumed to consist of stretched vortices whose orientations are determined by the resolved velocity field. An equation which relates the subgrid stress to the structure orientation and the subgrid kinetic energy, together with an assumed Kolmogorov energy spectrum for the subgrid vortices, gives a closed coupling of the SGS model dynamics to the filtered Navier–Stokes equations for the resolved flow quantities. The subgrid energy is calculated directly by use of a local balance between the total dissipation and the sum of the resolved-scale dissipation and production by the resolved scales. Simple one- and two-vortex models are proposed and tested in which the subgrid vortex orientations are either fixed by the local resolved velocity gradients, or rotate in response to the evolution of the gradient field. These models are not of the eddy viscosity type. LES calculations with the present models are described for 32^3 decaying turbulence and also for forced 32^3 box turbulence at Taylor Reynolds numbers R_λ in the range $R_\lambda \simeq 30$ (fully resolved) to $R_\lambda = \infty$. The models give good agreement with experiment for decaying turbulence and produce negligible SGS dissipation for forced turbulence in the limit of fully resolved flow. © *1997 American Institute of Physics.* [S1070-6631(97)02008-4]

I. INTRODUCTION

Despite the availability of large-scale scientific computing, direct numerical simulation (DNS) of the Navier–Stokes equations at Reynolds numbers typical of engineering application continues to remain beyond the reach of either present day facilities or those likely to be developed in the foreseeable future. This is because the range of scales that must be resolved in DNS increases very rapidly with increasing Reynolds number. The LES approach to this problem is to compute the detailed space and time dependence of the flow only at scales larger than some cutoff while modeling the effects on the retained scales of the transport of momentum and energy of the ''fine'' scales below the cutoff. The approach seems to be based on two related assumptions, first that the large (retained) scales are strongly coupled to the outer flow and the body geometry (boundary conditions) producing the turbulence, and second, that the ''fine'' scales exhibit a quasi-universal character with only weak dependence on the large scales. The task then remains of constructing subgrid models which are based in some sense on a physically realistic description of the fine scales.

Consider the large eddy simulation of the Navier–Stokes equations on a grid with a typical cell size of Δx and time step Δt. Let $\tilde{U}_i(\mathbf{x},t)$ represent the resolved (supergrid) velocity field and let $\tilde{P}(\mathbf{x},t)$ be the resolved pressure field. Put $U_i(\mathbf{x},t)=\tilde{U}_i(\mathbf{x},t)+u_i(\mathbf{x},t)$, where U_i is the full velocity field and u_i the subgrid field. The filtered LES equations for an incompressible fluid are

$$\frac{\partial \tilde{U}_i}{\partial x_i}=0, \tag{1}$$

$$\frac{\partial \tilde{U}_i}{\partial t}+\frac{\partial}{\partial x_j}(\tilde{U}_i\tilde{U}_j)=-\frac{\partial \tilde{P}}{\partial x_i}-\frac{\partial T_{ij}}{\partial x_j}-\frac{\partial L_{ij}}{\partial x_j}+\nu\frac{\partial^2 \tilde{U}_i}{\partial x_j \partial x_j}, \tag{2}$$

where

$$T_{ij}=\widetilde{u_i\tilde{U}_j}+\widetilde{u_j\tilde{U}_i}+\widetilde{u_iu_j}, \tag{3}$$

$$L_{ij}=\widetilde{\tilde{U}_i\tilde{U}_j}-\tilde{U}_i\tilde{U}_j. \tag{4}$$

Here T_{ij} is the subgrid stress tensor and L_{ij} is the Leonard stress tensor. The $\widetilde{u_iu_j}$ are the subgrid scale stresses which shall henceforth be denoted by τ_{ij}. Equations (1) and (2) are filtered equations over a discretized region of space; ''$\tilde{\ }$'' denotes the filtering operation defined using a kernel $G(\mathbf{x}-\mathbf{x}')$ such that

$$\tilde{U}_i(\mathbf{x},t)=\int G(\mathbf{x}-\mathbf{x}')U_i(\mathbf{x}',t)\,\mathbf{dx}'. \tag{5}$$

In principle L_{ij} can be evaluated given $\tilde{U}_i$ and G.[1,2] For the combination of a sharp cutoff spectral filter and a pseudo-spectral numerical method, both with the same spectral cutoff, $L_{ij}=0$. Since this is the method used presently, L_{ij} will not be discussed further. Evaluation of cross terms in the expression for T_{ij} appears to require detailed knowledge of u_i which LES seeks to avoid. We will presently lump the three terms of (3) together through $T_{ij}=\tau_{ij}$. This is not completely satisfactory but will be shown to produce a physically sensible class of models. A further complication concerns the question of filtering in time. At large Reynolds numbers Eqs. (1)–(4) appear to have little physical meaning on time-scales of the order $(\nu/\epsilon)^{1/2}$. Time-wise integration of (1)–(4) is usually done with time-step $\Delta t_L \gg (\nu/\epsilon)^{1/2}$, which implies a filter. This is important for our physical interpretation of the present model.

The most popular subgrid stress (SGS) models used to date utilize the the Smagorinsky realization of the eddy-viscosity idea. The subgrid stresses are written as[3]

$$\tau_{ij}-\tfrac{1}{3}\delta_{ij}\tau_{kk}=-2(C\Delta)^2|\widetilde{S}|\widetilde{S}_{ij}, \tag{6}$$

where $\widetilde{S}_{ij}=(\partial\widetilde{U}_i/\partial x_j+\partial\widetilde{U}_j/\partial x_i)/2$ is the resolved rate-of-strain tensor, $|\widetilde{S}|^2=2\widetilde{S}_{ij}\widetilde{S}_{ij}$, and C is a dimensionless number called the Smagorinsky coefficient. Δ is some characteristic length scale, i.e., the scale below which (5) represents the effect of the averaged motion of the neglected scales. Values of C in the range 0.1–0.2 have been used. A difficulty with assuming C to be constant is that the eddy viscosity overwhelms the molecular viscosity in regions of laminar flow. In the ''dynamic model,''[4,5] this problem is handled by use of a procedure based on evaluating the Leonard stresses at various filter scales, together with certain kinematical identities to develop techniques for computing $C(\mathbf{x},t)$ as the LES computation proceeds. These and other developments in LES modeling are reviewed by Reynolds[6] and Lesieur.[7]

In what follows, we develop in Sec. II, the main features of the present SGS models and show how coupling to the equations for the filtered quantities is achieved. The incorporation of the present models into a LES code is described in Sec. III A while Sec. III B and Sec. III C give details of the calculation of decaying turbulence and forced box turbulence respectively. An energy/dissipation evolution model for the subgrid vortices is discussed briefly in Sec. IV, as an alternative to the present method based on local balance arguments.

II. A VORTEX-BASED SUBGRID STRESS MODEL

A. Subgrid stresses and vortex orientation

We propose a structural model of the subgrid vorticity based on a stretched-vortex representation of the subgrid scales. Structure-based models designed for turbulence computation were discussed by Reynolds[8] and specific models have been proposed by Pullin and Saffman,[9] henceforth PS, aimed at SGS modeling for LES, and by Reynolds and Kassinos[10] in the context of one-point closure. The general approach may be characterized as *structure-based Reynolds stress closure*. Presently we implement and further develop the stretched-vortex subgrid model of PS. Here the subgrid vorticity consists of a superposition of vorticity fields or ''structures,'' each with the property that the vorticity is unidirectional, with no explicit dependence on the vorticity magnitude on the coordinate parallel to the vorticity. Some support for this structure is provided by the observed tendency, in several numerical simulations,[11,12] for alignment between the vorticity vector and the eigenvector corresponding to the algebraically intermediate principal rate-of-strain, thus suggesting a small-scale structure which is nearly ''two-dimensional,'' stretched by strain which is rather weaker than the small-scale vorticity. Special cases are the Burgers–Townsend vortex[13] and the Lundgren[14] stretched-spiral vortex, both of which have been applied to calculation of fine-scale turbulence properties.[15,16] The success of the stretched-vortex models of the fine scales, while mixed, does suggest that they may form the basis of a viable SGS model for LES. In what follows we give a description of the subgrid vortex orientation and an expression for the subgrid stresses. When combined with schemes for relating the vortex orientation and the subgrid turbulent energy to the resolved scales, a closed system of LES equations results.

Since the main problem of SGS modeling for LES is to represent the averaged effect of the small scales on the dynamics of the resolved scales, there is less need for a detailed subgrid vorticity distribution than is required by calculation of the fine scale properties themselves. Hence we use a simple, effectively axisymmetric model of a typical subgrid structure. PS showed that, under certain assumptions, in the sense of a random superposition of fields, the ensemble-averaged subgrid stresses of the vortex collection can be expressed in terms of the subgrid energy, $k>k_c$, as

$$\tau_{ij}=2\int_{k_c}^{\infty}E(k)\;dk\;\langle \mathsf{E}_{pi}\mathsf{Z}_{pq}\mathsf{E}_{qj}\rangle, \tag{7}$$

where

$$K\equiv\int_{k_c}^{\infty}E(k)\;dk \tag{8}$$

is the subgrid energy, $E(k)$ is the subgrid energy spectrum, E_{ij} is the rotation matrix for transformation from vortex-fixed to laboratory axes, Z_{ij} is a diagonal tensor with diagonal elements $(\frac{1}{2},\frac{1}{2},0)$, $\langle \mathsf{E}_{pi}\mathsf{Z}_{pq}\mathsf{E}_{qj}\rangle$ is a moment of the probability density function (pdf) $P(\alpha,\beta)$ of the Euler angles α and β describing the orientation of the subgrid vortex axis relative to laboratory axes (see PS equation (7) and (8)), and k_c is a cutoff wavenumber. The ensemble average over Euler angles is defined as

$$\langle f(\mathsf{E}_{ij})\rangle=\frac{1}{4\pi}\int_0^{\pi}\int_0^{2\pi}f(\mathsf{E}_{ij})P(\alpha,\beta)\sin\alpha\;d\alpha\;d\beta. \tag{9}$$

PS give several derivations of (7). The simplest asserts that in the frame of reference fixed in a vortex, with the ''3'' direction, or vortex axis, aligned with the vorticity, the energy associated with the vorticity must be equipartitioned in the two directions normal to this axis. The internal and unknown vorticity distribution need not be axisymmetric. Equation (7) holds for an arbitrary internal vorticity distribution in an individual structure following averaging over spin angles γ about the vortex axis, when γ is assumed uniformly distributed in $0\leqslant\gamma\leqslant 2\pi$. Equation (7) is nevertheless operationally equivalent to an axisymmetric subgrid vortex. We justify this by arguing that at sufficiently large Reynolds number and for sufficiently small k_c, the subgrid vortex dynamics may be assumed to be evolving on a time scale which is fast compared to Δt_L, the integration time step for (1)–(4). In Δt_L either some degree of subgrid dynamic axisymmetrization can be expected, or, alternatively owing to its self-induced motion about its axis, some azimuthal averaging, equivalent to a sampling of the space of state spin angles, will occur, thus giving a tendency to equipartition. We remark that (7) has a similar structure to the ''dimensionality tensor'' of Reynolds.[8]

Calculation of τ_{ij} from (7) requires both K and the distribution of structure orientations. PS proposed that the sub-

grid vortex structures are convected and rotated by the resolved field. The equation describing the evolution of $P(\alpha,\beta)$ is then

$$\frac{\partial P}{\partial t}+\widetilde{U}_j\frac{\partial P}{\partial x_j}+\frac{1}{\sin\alpha}\frac{\partial}{\partial\alpha}(\widetilde{U}_\alpha\sin\alpha P)+\frac{1}{\sin\alpha}\frac{\partial}{\partial\beta}(\widetilde{U}_\beta P)=0, \tag{10}$$

where $\widetilde{U}_\alpha$ and $\widetilde{U}_\beta$ are the projections of the resolved field $r_j\partial\widetilde{U}_i/\partial x_j$ onto the unit sphere. The third and fourth terms of (10) give the contribution to the rate of change of P from rotation by $\partial\widetilde{U}_i/\partial x_j$. The use of (10) is justified by heuristic appeal to the ideas of rapid distortion theory in the context of the present structural model. In the cells, individual vortices feel the local strain provided by the resolved field and rotate in response. In the PS model, the subgrid energy was determined by assuming that $E(k)$ had a locally Kolmogorov form. The local dissipation ϵ was calculated by relating it to the sum of the local production plus the local dissipation in the resolved field. This model, with appropriate boundary conditions for P, gives closure. It is not of the eddy-viscosity type.

B. Vortex orientation models

We tried to solve (10) using an ellipsoidal model for $P(\alpha,\beta)$. This was unsuccessful as it was found that the ellipsoid rapidly evolved into a ''cigar'' irrespective of its initial conditions. This is consistent with the analysis of Cocke[17] and later Orszag,[18] who showed that for homogeneous isotropic turbulence the length of a material line always increases on the average with time. This led us to the natural choice of delta-function pdf models. Presently we describe an approach based on modeling $P(\alpha,\beta)$ by product delta functions or a linear combination of products of delta functions. Typically we have

$$P(\alpha,\beta)=\frac{4\pi}{\sin\alpha}\,\delta(\alpha-\theta)\,\delta(\beta-\phi)\equiv\wp(\mathbf{e}|\mathbf{e}^v), \tag{11}$$

where $\theta(\mathbf{x},t)$, $\phi(\mathbf{x},t)$ is the specific orientation, and where the unit vectors $\mathbf{e}$ and $\mathbf{e}^v$ are defined respectively by

$$e_1=\sin\alpha\cos\beta,\quad e_2=\sin\alpha\sin\beta,\quad e_3=\cos\alpha, \tag{12}$$

$$e_1^v=\sin\theta\cos\phi,\quad e_2^v=\sin\theta\sin\phi,\quad e_3^v=\cos\theta. \tag{13}$$

We have introduced the notation $\wp(\mathbf{e}|\mathbf{e}^v)$ for convenience. While, this almost certainly oversimplifies the subgrid vortex dynamics, the spirit of LES is to obtain the averaged effect of subgrid motions on resolved scales, and it is hoped that (11) will suffice for this purpose.

It then follows from (11) that Eq. (7) can be written as

$$\tau_{ij}=(\delta_{ij}-e_i^ve_j^v)\int_{k_c}^{\infty}E(k)\,dk. \tag{14}$$

We now describe some specific orientation models used presently. The first two align the vortices with directions defined by the local resolved strain rates. We refer to these as *local alignment models*. They are simple and easy to implement. The third model attempts to couple the vortex orientation to the evolution of the resolved rate-of-strain tensor.

1. Model 1a: Alignment with $\tilde{\mathbf{e}}_3$ and $\tilde{\mathbf{e}}_2$

This model, proposed by PS, is based on the idea that the subgrid structures respond on a fast time scale to the supergrid strain. Let the eigenvectors of $\widetilde{S}_{ij}$ be $\widetilde{\mathbf{e}}_1$, $\widetilde{\mathbf{e}}_2$, and $\widetilde{\mathbf{e}}_3$, corresponding to eigenvalues $\lambda_1<\lambda_2<\lambda_3$, such that $\lambda_1+\lambda_2+\lambda_3=0$. It is assumed that a fraction of the local subgrid structures tend to become aligned with $\widetilde{\mathbf{e}}_3$ and the remainder align with the intermediate eigenvector $\widetilde{\mathbf{e}}_2$. The orientation pdf is a two-vortex model given by

$$P(\mathbf{e})=\lambda\wp(\mathbf{e}|\widetilde{\mathbf{e}}_3)+(1-\lambda)\wp(\mathbf{e}|\widetilde{\mathbf{e}}_2), \tag{15}$$

where

$$\lambda=\frac{\lambda_3}{|\lambda_2|+\lambda_3}. \tag{16}$$

With equipartition of subgrid energy among the vortices, τ_{ij} is given by

$$\tau_{ij}=[\lambda(\delta_{ij}-\widetilde{e}_{3i}\widetilde{e}_{3j})+(1-\lambda)(\delta_{ij}-\widetilde{e}_{2i}\widetilde{e}_{2j})]\times\int_{k_c}^{\infty}E(k)\,dk. \tag{17}$$

2. Model 1b: Alignment with $\tilde{\mathbf{e}}_3$ and the resolved vorticity vector, $\tilde{\omega}$

Model 1a will be later shown to contain no backscatter, i.e., the subgrid structures are subject only to stretching. In order to allow for backscatter we propose the model

$$P(\mathbf{e})=\mu\wp(\mathbf{e}|\widetilde{\mathbf{e}}_3)+(1-\mu)\wp(\mathbf{e}|\mathbf{e}^\omega), \tag{18}$$

$$\tau_{ij}=[\mu(\delta_{ij}-\widetilde{e}_{3i}\widetilde{e}_{3j})+(1-\mu)\times(\delta_{ij}-e_i^\omega e_j^\omega)]\int_{k_c}^{\infty}E(k)\,dk, \tag{19}$$

where $(1-\mu)$ is the fraction of structures aligned with the resolved vorticity, with direction $e_j^\omega=\widetilde{\omega}_j/|\widetilde{\omega}|$, where $\widetilde{\omega}$ is the resolved vorticity. This model is arbitrary but can be shown to include backscatter. As partial justification we note that we should expect complete alignment with $\widetilde{\omega}$ in the DNS limit. We have performed calculations with $\mu=0,0.5,1.0$.

3. Model 2: Rotation by $\tilde{A}_{ij}$

The *local alignment models* make no use of (10). A realizable model intermediate in complexity between (10) and Models 1a and b can be obtained by substituting (11) into (10) and using (13) to yield

$$\frac{\partial e_i^v}{\partial t}=e_j^v\widetilde{A}_{ij}-e_i^ve_k^ve_j^v\widetilde{A}_{kj}, \tag{20}$$

where

$$\widetilde{A}_{ij}\equiv\frac{\partial\widetilde{U}_i}{\partial x_j} \tag{21}$$

is the resolved velocity-gradient tensor; see the Appendix for an alternative derivation. In practice, owing to the need for

dealiasing arising in the implementation of spectral methods, it is more convenient to work with the equation for a vector defined by $l_i = Q(\mathbf{x},t)e_i^v$. If $Q(\mathbf{x},t)$ is chosen such that l_1 is a solenoidal field, Eq. (20) can be written as

$$\frac{\partial l_i}{\partial t} - \frac{\partial}{\partial x_j}(l_j \tilde{U}_i) = 0. \tag{22}$$

It is straightforward to show that the axis of a straight compact vortex, with an arbitrary internal vorticity distribution, when embedded in a time-dependent outer strain field, will rotate according to Eq. (20). We remark that in obtaining (22) we have omitted convection of the subgrid vortices by the resolved field. This is somewhat unsatisfactory but is done owing to the ill-posedness produced by convection. An alternative is to introduce a model damping mechanism, which we wish to avoid.

C. Subgrid energy and dissipation

Closure of all the aforementioned models requires knowledge of the subgrid energy K. Our present method of evaluating K invokes a local balance between the total dissipation and the sum of the resolved-scale dissipation and the production of turbulent kinetic energy by the interaction between the resolved rate-of-strain tensor and the subgrid stresses. An alternative approach based on $K-\epsilon$-type equations for the subgrid vortices is discussed in Sec. IV but is not implemented presently.

We develop the local balance arguments for the *rotation model*; they can be *mutatis mutandis* carried out for the alignment models 1a and 1b, respectively. It is assumed that the difference between the total local dissipation, ϵ, and the resolved-scale viscous dissipation is in balance with the local supergrid energy production, $\varepsilon_{\mathrm{sgs}}$, so that

$$\epsilon = 2\nu \tilde{S}_{ij}\tilde{S}_{ij} + \varepsilon_{\mathrm{sgs}}, \quad \varepsilon_{\mathrm{sgs}} \equiv -\tilde{S}_{ij}\tau_{ij} = -K\tilde{S}_{ij}\left(\delta_{ij} - \frac{l_i l_j}{l_m l_m}\right). \tag{23}$$

Closure is obtained by assuming a Kolmogorov form of $E(k)$ with a viscous cutoff

$$\begin{aligned} E(k) &= \mathscr{K}_0 \epsilon^{2/3} k^{-5/3}, \quad && k_c < k < \eta^{-1}, \\ &= 0, && k > \eta^{-1}, \end{aligned} \tag{24}$$

where $\mathscr{K}_0$ is the Kolmogorov prefactor and $\eta = (\nu^3/\epsilon)^{1/4}$ is the local Kolmogorov length. We remark that for stretched vortex models of the fine scales $E(k)$ depends only on the internal structure of the vorticity and is independent of $P(\mathbf{e})$;[9,14] there is no assumption of isotropy and therefore no inconsistency in combining a Kolmogorov spectrum with local anisotropy. Alternatives to the sharp dissipation cutoff of (24) would be to assume that each subgrid vortex is of the Lundgren spiral vortex form, and to replace (24) with the Lundgren spectrum, or to use an exponential cutoff near $k\eta = 1$ as suggested by DNS[19]/and experiment.[20] The sharp cutoff is chosen presently for simplicity; at large Reynolds numbers the energy integral converges absolutely when (24) is used and $\nu \to 0$. At low Reynolds number, the model subgrid stresses are subdominant to the resolved viscous stresses (see PS, Appendix B). The actual form of the dissipation range $E(k)$ would be important if one were trying to predict the distribution of the dissipation across the subgrid scales, but the spirit of LES is to get the averaged effects, without having to compute all the subgrid details, and we expect a simple model to be sufficient for this purpose. We remark that (24) can be viewed as introducing a cutoff parameter $k\eta = J$, where we have chosen $J = 1$. Finally, it might be objected that (24) is inconsistent with the effective axisymmetric vortex structure. We again emphasize the PS kinematic derivation of (7) is for an arbitrary internal vorticity distribution when the average over uniformly distributed spin angles is allowed.

Using (24) in (14) the subgrid stresses may be expressed as

$$\begin{aligned} \tau_{ij} &= \frac{3.\mathscr{K}_0}{2k_c^{2/3}} \epsilon^{2/3}(1-(k_c\eta)^{2/3})\left(\delta_{ij} - \frac{l_i l_j}{l_m l_m}\right), \quad && k_c\eta < 1, \\ &= 0, \quad && k_c\eta > 1. \end{aligned} \tag{25}$$

When Eq. (25) is substituted in Eq. (23) one obtains

$$\begin{aligned} \epsilon &= 2\nu \tilde{S}_{ij}\tilde{S}_{ij} - \frac{3.\mathscr{K}_0}{2k_c^{2/3}} \epsilon^{2/3}(1-(k_c\eta)^{2/3}) \\ &\quad \times \tilde{S}_{ij}\left(\delta_{ij} - \frac{l_i l_j}{l_m l_m}\right), \quad k_c\eta < 1, \\ &= 2\nu \tilde{S}_{ij}\tilde{S}_{ij}, \quad k_c\eta > 1, \end{aligned} \tag{26}$$

which, upon using the transformation

$$X = k_c\eta = k_c\left(\frac{\nu^3}{\epsilon}\right)^{1/4}, \tag{27}$$

gives

$$\begin{aligned} &1 - \hat{S}_1 X^4 + 3.\mathscr{K}_0 \hat{S}_2 X^{4/3}(1-X^{2/3}) = 0, \quad X < 1, \\ &1 - \hat{S}_1 X^4 = 0, \quad X > 1, \end{aligned} \tag{28}$$

where

$$\hat{S}_1 = \frac{2\tilde{S}_{ij}\tilde{S}_{ij}}{k_c^4 \nu^2}, \tag{29}$$

$$\hat{S}_2 = \tilde{S}_{ij}\frac{(\delta_{ij} - l_i l_j/l_m l_m)}{2k_c^2 \nu}. \tag{30}$$

It can be shown that for $\hat{S}_1 > 0$ (28) always has a positive real root. It will later be demonstrated that (28) can have multiple solutions for X in certain regions of $\hat{S}_1 - \hat{S}_2$ space, but these will be seen to be well removed from realizable values of $\hat{S}_1$, $\hat{S}_2$. The required solution is defined as that on a continuous branch from the positive solution corresponding to $\hat{S}_2 = 0$. When $\hat{S}_1 < 1$ this can be shown to satisfy $X > 1$, which from (25) gives zero subgrid stresses, while for $\hat{S}_1 > 1$ this branch gives $X < 1$ always. Hence in practice the first of (28) is solved only when $\hat{S}_1 > 1$; otherwise the SGS model turns off, or, equivalently, we set $X = 1$. This corresponds to locally fully resolved flow.

For the defined branch, dominant balance arguments can be used to show that in the limit of $\nu \to 0$

$$\epsilon = \frac{27\mathscr{K}_0^3}{8k_c^2}\left(-\widetilde{S}_{ij}\left(\delta_{ij}-\frac{l_i l_j}{l_m l_m}\right)\right)^3, \quad \hat{S}_2<0 \tag{31}$$

$$=0, \quad \hat{S}_2>0. \tag{32}$$

Equation (28) is our basic result for calculating the dissipation, from which the subgrid stresses follow from (25). Presently we use (28) in two different implementations. In the first, $\mathscr{K}_0$ is specified as a parameter and is held fixed for the simulation. This is the *fixed* $\mathscr{K}_0$ scheme. In the second implementation, $\mathscr{K}_0$ is calculated dynamically as follows; label the points in physical space at which the resolved field is calculated by index $m=1,\ldots,M$, where, for example, $M=N^3$ for an N^3 spectral method. Next, write (28) at each point of the resolved flow in physical space as

$$H(\hat{S}_{1,m}-1)(1-\hat{S}_{1,m}X_m^4+3.\mathscr{K}_0\hat{S}_{2,m}X_m^{4/3}(1-X_m^{2/3}))$$

$$+H(1-\hat{S}_{1,m})(1-X_m)=0, \quad m=1,\ldots,M, \tag{33}$$

where $H(\ldots)$ denotes the Heaviside function, $X_m=k_c(\nu^3/\epsilon_m)^{1/4}$, ϵ_m being the local dissipation at point m, and $\hat{S}_{1,m}$, $\hat{S}_{2,m}$ are (29) and (30) evaluated at point m.

Now let $\widetilde{E}(\widetilde{k})$ be the energy spectrum of the resolved field at some specified wavenumber $k=\widetilde{k}$, $\widetilde{k}<k_c$. Assume that $\widetilde{E}(\widetilde{k})$ conforms to (24),

$$\widetilde{E}(\widetilde{k})=\mathscr{K}_0\langle\epsilon\rangle^{2/3}\widetilde{k}^{-5/3}, \tag{34}$$

where $\langle\epsilon\rangle$ is the instantaneous volume-averaged dissipation, which can be expressed as

$$\langle\epsilon\rangle=\frac{1}{M}\sum_{m=1}^{M} H(\hat{S}_{1,m}-1)\,\frac{\nu^3k_c^4}{X_m^4}+H(1-\hat{S}_{1,m})2\nu\widetilde{S}_{ij}\widetilde{S}_{ij}. \tag{35}$$

Equation (34) forces continuity of the resolved and subgrid energy spectra at $k=\widetilde{k}$, which in practice is chosen near to, but somewhat less than, k_c. Eliminating $\langle\epsilon\rangle$ from (34) and (35) gives

$$\frac{\hat{F}}{\mathscr{K}_0^{3/2}}-\frac{1}{M}\sum_{m=1}^{M} H(\hat{S}_{1,m}-1)\,\frac{1}{X_m^4}+H(1-\hat{S}_{1,m})\hat{S}_{1,m}=0, \tag{36}$$

where

$$\hat{F}=\frac{\widetilde{E}^{3/2}\widetilde{k}^{5/2}}{\nu^3k_c^4}. \tag{37}$$

When M, k_c, $\widetilde{k}$, $\widetilde{E}$, ν, and $\hat{S}_{1,m}$, $\hat{S}_{2,m}$ are given, (33) and (36) are $M+1$ nonlinear equations for X_m $(m=1,\ldots,M)$ and $\mathscr{K}_0$. Once the X_m are known, the ϵ_m can be calculated and the subgrid stresses follow from (25) applied at each point. We refer to this as the *coupled* $\mathscr{K}_0$ scheme. The methods by which the *fixed* $\mathscr{K}_0$ and the *coupled* $\mathscr{K}_0$ schemes are incorporated into a LES code are described in the next section.

III. FORCED AND DECAYING ISOTROPIC TURBULENCE

A. Numerical method

We consider an incompressible fluid in a cubical box of length 2π. We solve (1) and (2) with and without a forcing term, coupled with (22) (for the rotation model), using periodic boundary conditions in all three directions. In Fourier space (1) and (2) may be combined to give (subscript **k** has been dropped)

$$\frac{\partial\hat{\widetilde{U}}_i}{\partial t}=-\nu k^2\hat{\widetilde{U}}_i+\mathscr{P}[-(ik_j\widehat{\widetilde{U}_i\widetilde{U}_j})-(ik_m\hat{T}_{im})+\hat{f}_i], \tag{38}$$

where $\mathscr{P}$ is the projection operator on the space of solenoidal fields, defined as

$$\mathscr{P}=\delta_{ij}-\frac{k_ik_j}{k^2}. \tag{39}$$

In k-space (22) is

$$\frac{\partial\hat{l}_i}{\partial t}-ik_j\widehat{l_j\widetilde{U}_i}=0. \tag{40}$$

A Fourier–Galerkin pseudo-spectral method is used with ''3/2 de-aliasing rule'' for the nonlinear terms both in the momentum and subgrid equations, that is 32 Fourier modes in each direction are advanced in time; the computation of the nonlinear terms where done using 48 modes, the extra 16 modes used for padding. A second-order explicit Runge–Kutta scheme is used for time advancement.

The rotation model is incorporated into the LES code as follows; equations (1), (2), (14), and (22) are solved simultaneously for the fields $\widetilde{U}_i$ and l_i. At a given time-step (or intermediate time-step) the l_i are obtained from the Fourier coefficients $\hat{l}_i$ which allows construction of the rotation matrix $\mathsf{E}_{ij}(\mathbf{x})$ and hence the contractions $\hat{S}_1$ and $\hat{S}_2$. For the *fixed* $\mathscr{K}_0$ scheme, in which $\mathscr{K}_0$ is a specified parameter, Eq. (28) is solved for X_m individually at each of 32^3 points using Newton–Raphson, whence $\epsilon(\mathbf{x})$ follows from (27) and $\tau_{ij}(\mathbf{x})$ from (25). This is transformed back to Fourier space and fed into the momentum equation. In the *coupled* $\mathscr{K}_0$ scheme, the scalar solution of (28) is replaced by simultaneous solution of (33) and (36), which gives both $\mathscr{K}_0$ and the dissipation field. We note that the Jacobian of the coupled nonlinear system is diagonal with single sidebands, thus the linear equations which result from application of the Newton–Raphson method can be solved directly in order $M=32^3$ operations.

The *local alignment* models operate similarly but do not require solution of (22) since $\hat{S}_1$ and $\hat{S}_2$ can be calculated directly from resolved flow variables. Some extra computation is involved is solving the scalar equation in each cell to obtain the eigenstates of $\widetilde{S}_{ij}$. We used the initial approximation $X=\hat{S}_1^{-1/4}$, $\hat{S}_2<0$, and, from dominant balance, $X=2.0$, $\hat{S}_2>0$. This itself can be avoided if (31) is used, but this was found to produce a somewhat overly dissipative model in the DNS limit; see discussion below. A choice of

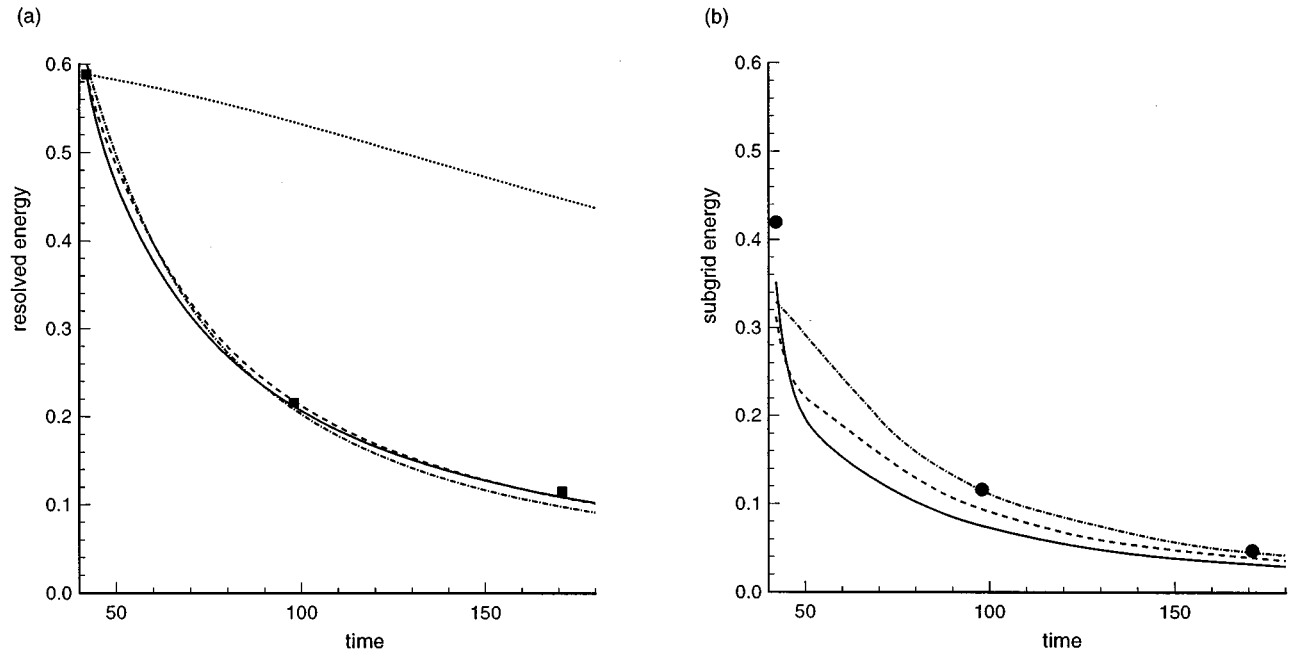

FIG. 1. Decay of the resolved (a) and the subgrid (b) energy. Solid line—C-$\mathscr{K}_0$[1a], dashed line—C-$\mathscr{K}_0$[1b;0.5], dot—dashed line—C-$\mathscr{K}_0$[2], and dotted line—no model. The symbols are data from Ref. 21.

$\mathscr{K}_0=1.5$ is used as an initial guess for flows with $R_\lambda>80$; for lower Reynolds number one needs to lower this initial guess to obtain convergence.

The results presented in Sec. III B are obtained using the *coupled* $\mathscr{K}_0$ scheme. The *fixed* $\mathscr{K}_0$ scheme gives almost identical results with the appropriate value of $\mathscr{K}_0$ chosen. In Sec. III C we present results from all the models in forced turbulence. The *fixed* $\mathscr{K}_0$ scheme will be referred to by F-$\mathscr{K}_0$[...] and the *coupled* $\mathscr{K}_0$ scheme by C-$\mathscr{K}_0$[...]. The bracketed information indicates the model number, i.e., 1a, 1b, or 2. For example, F-$\mathscr{K}_0$[1a] would refer to *model 1a* with $\mathscr{K}_0$ held fixed while C-$\mathscr{K}_0$[1b;0.5] would refer to *model 1b* with $\mu=0.5$ using the *coupled* $\mathscr{K}_0$ scheme.

B. Decaying turbulence

We study decaying isotropic turbulence in order to compare our results to the experiment of Comte-Bellot and Corrsin.[21] They measured the energy spectrum at three downstream locations in grid turbulence. One can relate this to decaying isotropic turbulence by invoking the Taylor approximation. We mimic their experiment by studying turbulence in a cubical box with periodic boundary conditions. In a frame of reference moving with the mean flow speed,

$$t=\int_0^x \frac{dx'}{\overline{U(x')}}, \tag{41}$$

where x is the downstream distance from the grid and $\overline{U(x)}$ is the mean flow velocity over the cross section of the tunnel. We have nondimensionalized the experimental data by the following characteristic velocity, length and time scales: $U_{\rm ref}=\sqrt{3U_0'^2/2}$, $L_{\rm ref}=L/2\pi$, and $t_{\rm ref}=L_{\rm ref}/U_{\rm ref}$. In their experiments the velocity fluctuation at the first measuring station is $\sqrt{U_0'^2}=22.2$ cm/s, the free-stream speed is $U_\infty=10^3$ cm/s, and the spacing of the turbulence generating mesh is $M_g=5.08$ cm. The size of the computational box, $L=11M_g$, was chosen to contain roughly four integral scales. The times at the three stations were measured in terms of $U_\infty t/M_g$. The initial Taylor Reynolds number is $R_\lambda\simeq 80$. In order to compare the resolved and the subgrid part of the turbulent energy produced by the computation, the measured spectra have been integrated over the relevant scale ranges. The results of this processing of the Comte-Bellot and Corrsin data was supplied to us by staff at the Center for Turbulence Research (CTR).

Figure 1(a) shows the decay of the resolved energy with time for all three models. The dotted line is the result of running the simulation with the model switched off. It is evident that the models play an important role in providing dissipation of kinetic energy. The decay of the subgrid energy with time is shown in Fig. 1(b). Note that the subgrid energy is obtained from the model without the solution of additional field equations. Since the subgrid energy is derived from knowledge of the resolved field and the chosen subgrid energy spectrum, it cannot be independently initialized to the match the experimental value. Figures 2(a) and 2(b) compare the resolved energy spectra with the measurements at the initial time and then at the two later instances. The initial spectrum is generated to match the experimental data, while the later two curves are the spectra calculated from the three models. Figure 1(a) gives the area under the curve of Figs. 2(a) and 2(b) at the three time instances, over the resolved range of scales. While all models give good agreement with the data for the decay of the resolved energy, C-$\mathscr{K}_0$[1a] and C-$\mathscr{K}_0$[1b;0.5] seem to give a slightly better resolved-scale spectrum than C-$\mathscr{K}_0$[2]. This may be related to an observed tendency for the power spectrum of the l_i for the rotation model (not shown) to peak towards the cutoff at

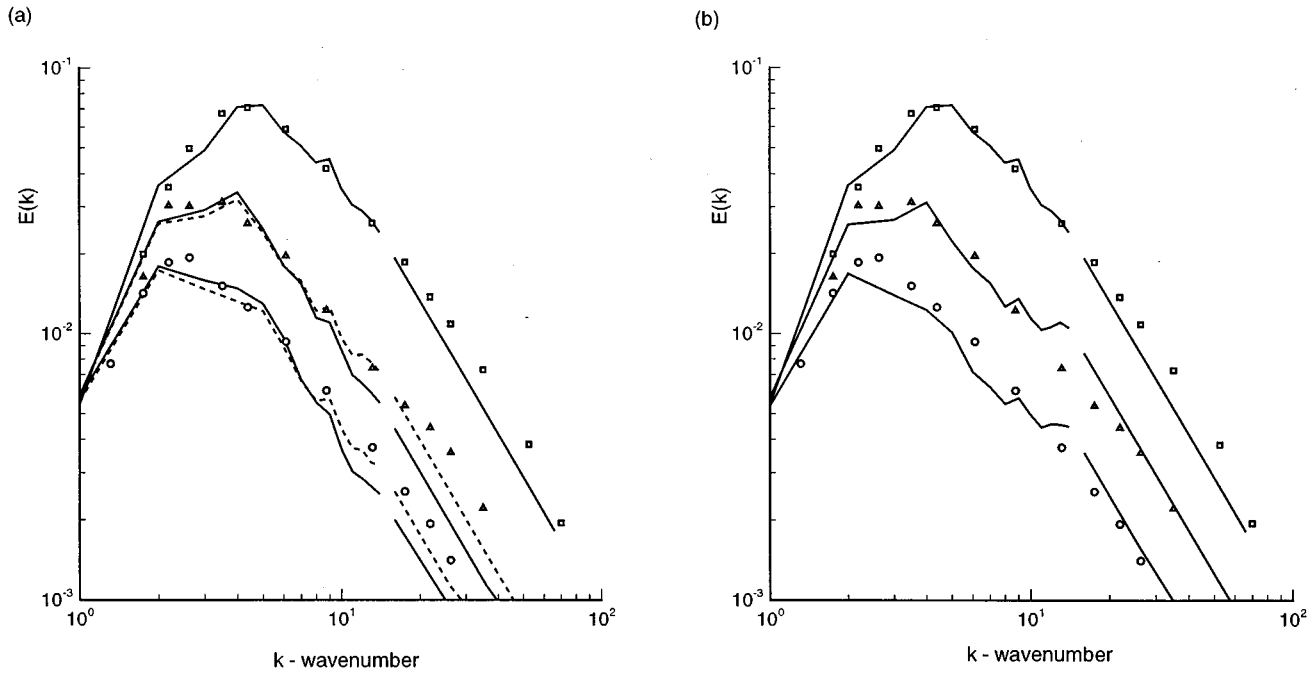

FIG. 2. Time evolution of spectra in decaying turbulence at three time instances. Solid line—C-$\mathscr{K}_0$[1a] and dashed line—C-$\mathscr{K}_0$[1b;0.5] (a) and C-$\mathscr{K}_0$[2] (b). The symbols are data from Ref. 21. The straight lines for $k>k_c$ are the calculated subgrid spectra.

k_c followed by a rapid decrease to zero at $k=k_c$. This apparently results from the nonlinear coupling between the l_i and the $\widetilde{U}_i$ fields, which in the absence of viscous damping produces a mild cascade towards higher wave numbers and a subsequent buildup near $k=k_c$. The response of the $\widetilde{U}_i$ field is seen to be a concomitant increase in $E(k)$ near the cutoff. The interaction between subgrid structures in adjacent cells occurs only implicitly via the LES equations and the subgrid stress relations. This is apparently too weak to adequately damp high wave number growth. Figure 3 shows the value of the Kolmogorov prefactor, $\mathscr{K}_0$, with time. The Kolmogorov prefactor $\mathscr{K}_0$ settles to about 1.5 for C-$\mathscr{K}_0$[1a], 1.85 for C-$\mathscr{K}_0$[1b;0.5], and hovers around 2.5 for the C-$\mathscr{K}_0$[2]. LES with C-$\mathscr{K}_0$[1b] for a range of values of μ were performed and yielded satisfactory results in the sense of agreement of the energy decay with experiment; $\mu=0$ resembled the rotation model in its behavior *vis à vis* the energy spectrum and the value of $\mathscr{K}_0$. Results in this paper will only be presented for the case $\mu=0.5$.

The computing time per time-step relative to the Smagorinsky model with constant C was found to be approximately 1.5 for models 1a and 1b and about 3 for the *rotation* model. The C-$\mathscr{K}_0$ scheme was marginally more expensive than the F-$\mathscr{K}_0$ scheme.

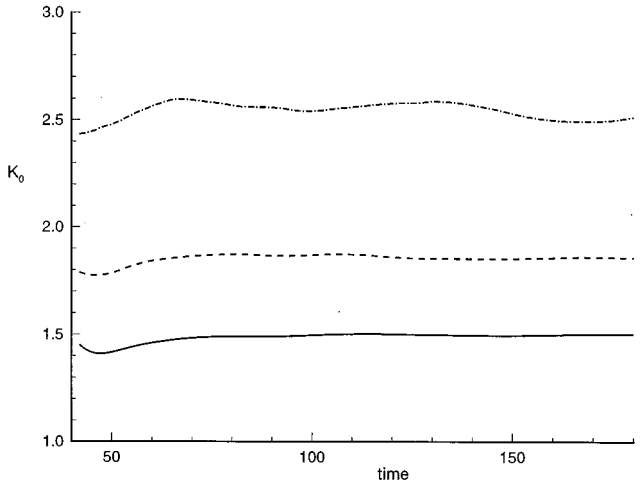

FIG. 3. Time variation of the Kolmogorov prefactor, $\mathscr{K}_0$, in decaying turbulence. solid line—C-$\mathscr{K}_0$[1a], dashed line—C-$\mathscr{K}_0$[1b;0.5], and dot–dashed line—C-$\mathscr{K}_0$[2].

C. Forced turbulence

Forcing is achieved by exciting low wave numbers such that the total energy injection rate is constant in time.[22] A certain selected number of Fourier modes are chosen from a wave number shell $|\mathbf{k}|=k_0$. The Fourier coefficient of the forcing term is then written as

$$\hat{\mathbf{f}}_k=\frac{\delta}{N}\frac{\widetilde{\widetilde{\mathbf{U}}}_k^*}{|\widetilde{\widetilde{\mathbf{U}}}_k^2|} \tag{42}$$

for all modes in the specified shell. The above choice of $\hat{\mathbf{f}}_k$ ensures that the energy injection rate, $\Sigma\,\hat{\mathbf{f}}_k\cdot\widetilde{\widetilde{\mathbf{U}}}_k$, is a constant and equal to δ. We have chosen $k_0=2$, $N=20$ (a box of side 2 grid units centered around the origin with the center modes and the origin left out) and $\delta=0.1$ for all the runs. The LES simulations with forcing were performed over a range of R_λ. The simulations run stably and eventually reach steady state when statistics are collected. Figure 4(a) shows a plot of

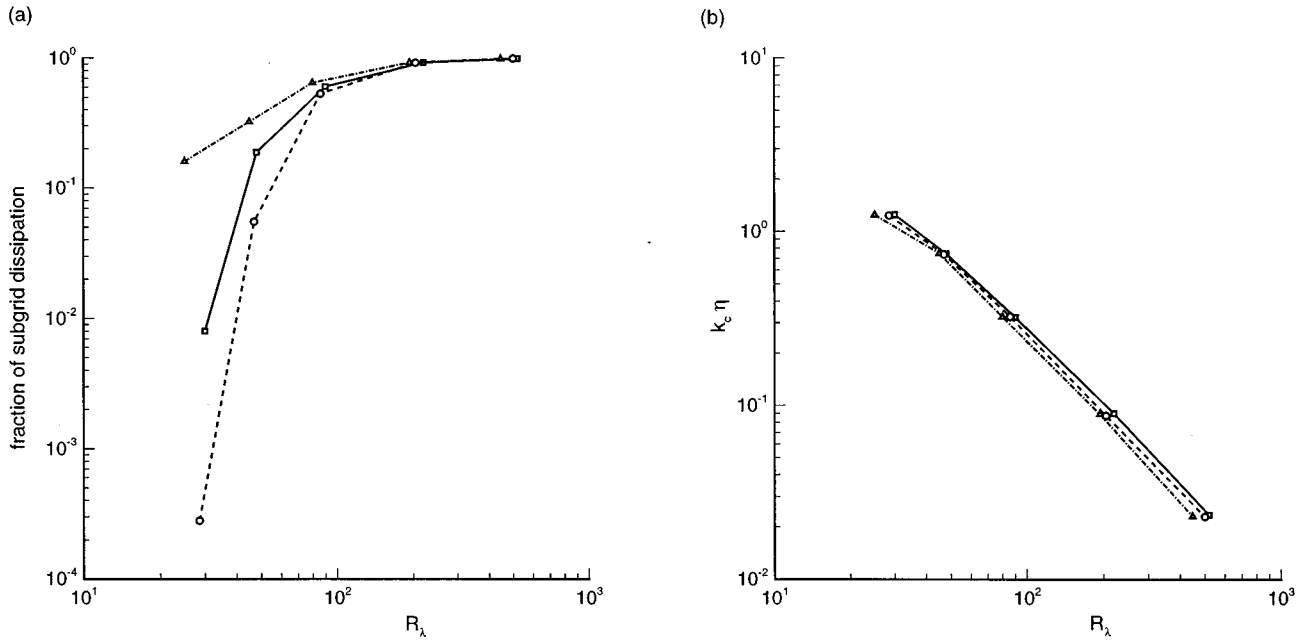

FIG. 4. $\langle \varepsilon_{\rm sgs}\rangle/\langle \epsilon\rangle$ versus R_λ (a) and $k_c\eta$ versus R_λ (b). Solid line—F-$\mathscr{K}_0$ scheme (models 1a, 1b, and 2 are indistinguishable), dashed line—C-$\mathscr{K}_0$ scheme (models 1a, 1b, and 2 are indistinguishable), and dot–dashed line—Smagorinsky model with $C=0.17$.

$\langle \varepsilon_{\rm sgs}\rangle/\langle \epsilon\rangle$, the ratio of the average subgrid dissipation to the total average dissipation in the box versus R_λ. The three curves shown are for the Smagorinsky model, the *fixed* $\mathscr{K}_0$ models and the *coupled* $\mathscr{K}_0$ models. For models incorporating the C-$\mathscr{K}_0$ scheme for forced turbulence, the computed values of $\mathscr{K}_0$ (not shown) showed an R_λ dependence that was somewhat model dependent. For each model $\mathscr{K}_0$ inceased with increasing R_λ from near zero at the DNS limit and reached a plateau for values of R_λ greater than about 100. These asymptotic, large R_λ values were 1.3, 1.5, and 2.0 for C-$\mathscr{K}_0$[1a], C-$\mathscr{K}_0$[1b;0.5], and C-$\mathscr{K}_0$[2], respectively, which we note are somewhat lower than the values shown in Fig. 3; this appears to be an R_λ effect. For the F-$\mathscr{K}_0$ calculations, these asymptotic $\mathscr{K}_0$ values were used for all R_λ. Figure 4(a) shows that the C-$\mathscr{K}_0$ models are less dissipative in the DNS limit than the F-$\mathscr{K}_0$ models and thus are superior in this respect. Figure 4(b) is a plot of $k_c\langle\eta\rangle$ vs R_λ, where here $\langle\eta\rangle=(\nu^3/\langle\epsilon\rangle)^{1/4}$, $\langle\epsilon\rangle$ being the box-averaged total dissipation. In both figures all results for the three models employing the same scheme were graphically indistinguishable. With 32^3 modes fully resolved DNS can be run at about $R_\lambda\simeq 25$. This was confirmed by turning off the SGS model and comparing computed values for the skewness and the flatness factors of the longitudinal velocity derivatives and one component of the vorticity with the results of Kerr[23] at the same resolution and similar R_λ. With the SGS models turned on we find $k_c\langle\eta\rangle=1$ at $R_\lambda\simeq 25$, indicating near full resolution except in the far viscous range. Figure 4(a) shows that the models are subdominant in this DNS limit, providing less than 0.0003 (C-$\mathscr{K}_0$) and 0.008 (F-$\mathscr{K}_0$), of the volume-averaged dissipation. By comparison, the Smagorinsky model produces a fraction 0.16 of the total dissipation at $R_\lambda\simeq 25$.

We remark that the simplest possible model of the present class can be constructed using vortex alignment with the eigenvector corresponding to λ_3 and (31) to evaluate $\varepsilon_{\rm sgs}$. At $R_\lambda\simeq 90$ this model performed similarly to model 1a for both decaying and homogeneous turbulence and was only marginally slower than Smagorinsky. It was found, like Smagorinsky, to be too dissipative in the DNS limit, and so is not discussed in detail.

The pdf of SGS in filtered DNS fields for both box turbulence[22] and nonhomogeneous flows[24] have typically shown some 30% backscatter. It follows from (23) that backscatter, defined by $\varepsilon_{\rm sgs}<0$, occurs whenever $\hat{S}_2>0$ while $\hat{S}_2<0$ gives cascade. A straightforward calculation using (23) shows that SGS dissipation can be written as

$$\begin{aligned}\varepsilon_{\rm sgs}&=-K\widetilde{S}_{ij}\left(\delta_{ij}-\frac{l_i l_j}{l_m l_m}\right)\\&\sim-\hat{S}_2K\\&=\overline{S'_{33}}K,\end{aligned}\tag{43}$$

where $\widetilde{S}'_{33}$ is the component of $\widetilde{S}_{ij}$ aligned with the vortex. Hence backscatter, defined by $\varepsilon_{\rm sgs}<0$, occurs whenever $\hat{S}_2>0$—the SGS vortices are being compressed on the average—while $\hat{S}_2<0$—the vortices are axially stretched—gives cascade. Figures 5(a)–5(c) show scatter plots of $\hat{S}_1$ vs $\hat{S}_2$ for the three orientation models obtained from a simulation at $R_\lambda\simeq 90$. Models incorporating the C-$\mathscr{K}_0$ or the F-$\mathscr{K}_0$ scheme exhibit similar behaviour. Model 1a has no backscatter (this can be demonstrated) while model 1b (with $\mu=0.5$) shows some ($\sim$3%) backscatter. The *rotation model* shows substantial backscatter, about $\sim$40%, and it is possible that this may be related to its somewhat higher computed values of $\mathscr{K}_0$ compared to models 1a and 1b. A simu-

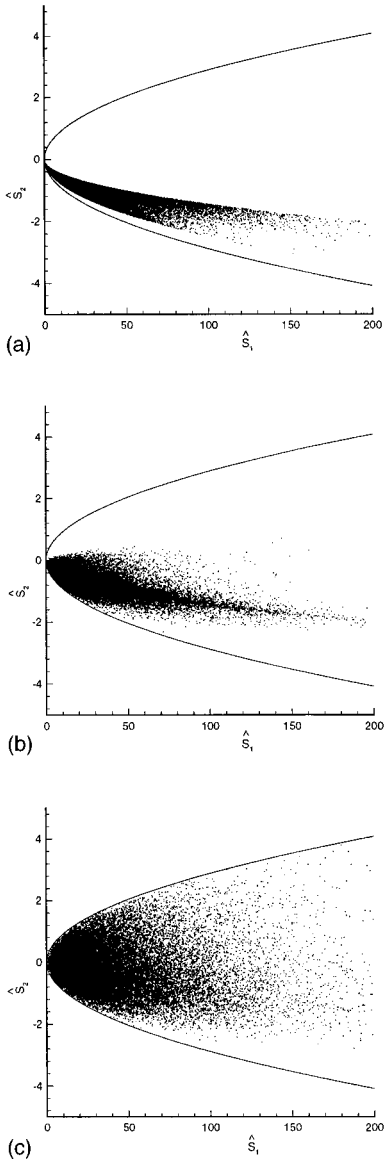

FIG. 5. Scatter plot of $\hat{S}_1$ vs $\hat{S}_2$ indicating regions of backscatter. F-$\mathscr{K}_0$[1a] (a) shows no backscatter, F-$\mathscr{K}_0$[1b;0.5] (b) shows some backscatter, and F-$\mathscr{K}_0$[2] (c) shows about 40% backscatter. The C-$\mathscr{K}_0$ models exhibit similar behavior.

lation with C-$\mathscr{K}_0$[1b;0], i.e., full alignment with the vorticity, show a similar scatterplot to C-$\mathscr{K}_0$[2]. This suggests a strategy of adjustment of μ to obtain backscatter agreeing with filtered DNS. It is interesting to note that the all points lie within a bounding parabola. An estimate based on a locally two-dimensional ''maximum stretch'' scenario for $\hat{S}_{ij}$ gives a bounding parabola $\hat{S}_1 = 16\hat{S}_2^2$. We find, however, that $\hat{S}_1 = 12\hat{S}_2^2$ gives a slightly better boundary and so this curve is displayed in the figures. The backscatter properties of the models are also illustrated in Fig. 6 which shows shows a pdf of the ''stretch,'' that part of the velocity gradient-tensor which stretches the subgrid vorticity. The stretch is suitably normalized by $\sqrt{\langle \epsilon \rangle / \nu}$. The pdf of the dissipation $\log_{10} \epsilon / \langle \epsilon \rangle$ for the three models is displayed in Fig. 7. The distribution appears to be approximately log-normal.

It was remarked earlier that (28) can exhibit regions of multiple roots in the $\hat{S}_2$ vs $\hat{S}_1$ plane, posing a potential problem in obtaining a unique value of ϵ, given $\hat{S}_1$, $\hat{S}_2$. This can be shown to occur only when $\hat{S}_2 < 0$. The boundary of the region corresponding to multiple-valuedness of $X(\hat{S}_1, \hat{S}_2)$ in the $\hat{S}_1$, $\hat{S}_2$ plane always lies well away from populated regions of the scatter-plots of Fig. 5. In fact, when $\hat{S}_1 \gg 1$, this boundary is given by $\hat{S}_2 \approx -256\hat{S}_1/(81\mathscr{K}_0)$, which lies well below the parabola bounding the scatter plots.

IV. CONCLUDING REMARKS

Stretched-vortex SGS models have been shown to perform well for both decaying and forced isotropic turbulence, over a range of R_λ. They give the subgrid energy directly and appear to produce the correct fully resolved flow in the DNS limit with computational penalty, for the alignment models, of some 50% in comparison to the standard Smagorinsky model. The F-$\mathscr{K}_0$ models are simple to implement and give satisfactory performance. The C-$\mathscr{K}_0$ approach allows dynamic calculation of $\mathscr{K}_0$ at the expense of some extra complexity. All variations of the model tested presently gave good comparison with data for decaying turbulence. The stretched-vortex models have been shown to produce backscatter, but none of the three tested give, in a natural way, the 30% backscatter seen in filtered DNS of isotropic turbulence. At the expense of adjusting μ, the fraction of subgrid vortices aligned with the resolved vorticity, a two-vortex alignment model with the right properties could be constructed but we have not done so presently. We remark that models incorporating the F-$\mathscr{K}_0$ scheme are fully constructed in physical space and thus are amenable to finite difference computations with complex flow geometries. The present C-$\mathscr{K}_0$ scheme is implemented in Fourier space, but this method could be used in physical space by replacing (34) with its second-order structure function equivalent

$$\overline{(\Delta u)^2} = f\mathscr{K}_0 \epsilon^{2/3} r^{2/3}, \tag{44}$$

where $\overline{(\Delta u)^2}$ is a measure of the shell-averaged (physical space) longitudinal velocity difference squared, and where $f = 1.31512$. This could be applied either globally with $\epsilon^{2/3}$ replaced by $\langle \epsilon^{2/3} \rangle$ or locally, with $r = \Delta$, where Δ is the local node spacing.

One could replace the local balance model of Sec. II C, including the assumption of a Kolmogorov energy spectrum, with transport equations for the subgrid vortex itself. The relevant equations for the subgrid energy K and the subgrid dissipation $\epsilon_{\rm sgs}$ arising from internal SGS vortex motions can be obtained from a model of a vortex moving evolving in a linear background field (see the Appendix)

$$\begin{aligned} \frac{DK}{Dt} &= -\widetilde{S}_{ij}\tau_{ij} - \epsilon_{\rm sgs} \\ &= -K\widetilde{S}_{ij}\left(\delta_{ij} - \frac{l_i l_j}{l_m l_m}\right) - \epsilon_{\rm sgs} \\ &= \widetilde{S}'_{33} K - \epsilon_{\rm sgs} \end{aligned} \tag{45}$$

and

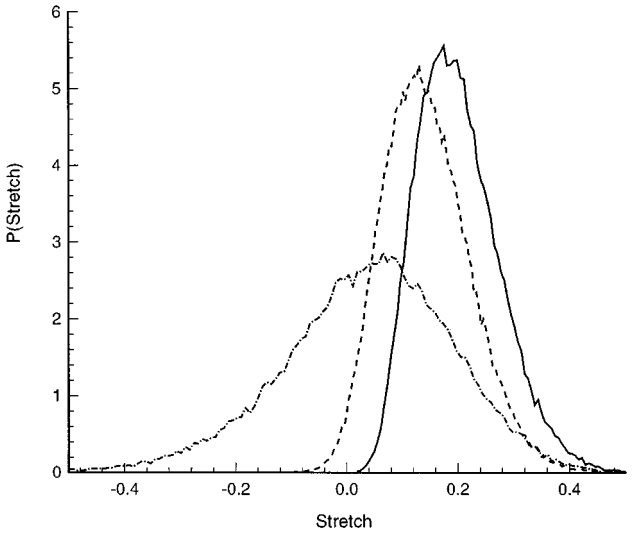

FIG. 6. The pdf of the ''stretch''—$\omega_i' \partial \tilde{U}_i / \partial x_j \omega_j'$. Solid line—F-$\mathscr{K}_0$[1a], dashed line—F-$\mathscr{K}_0$[1b;0.5], and dot–dashed line—F-$\mathscr{K}_0$[2]. The C-$\mathscr{K}_0$ models exhibit similar behavior.

$$\frac{D\epsilon_{\rm sgs}}{Dt} = 2\frac{l_i l_j}{l_k l_k}\tilde{S}_{ij}\epsilon_{\rm sgs} - 4\nu^2 \int_{k_c}^{\infty} k^4 E(k)\, dk, \tag{46}$$

where $\epsilon_{\rm sgs}$ is

$$\epsilon_{\rm sgs} \equiv 2\nu \int_{k_c}^{\infty} k^2 E(k)\, dk. \tag{47}$$

The first term on the right of (46) gives the increase of the subgrid enstrophy, and hence the dissipation, produced by local vortex stretching provided by the resolved scales, while the second term gives the effect of viscous diffusion of enstrophy. These equations can replace the local balance model for the computation of K; the stresses are still given by (14). The $K-\epsilon_{\rm sgs}$ are not closed, however, since $E(k)$ appears in (46). Closure can be obtained by applying a time filter to (45) and (46) and using the well-known approximate relation

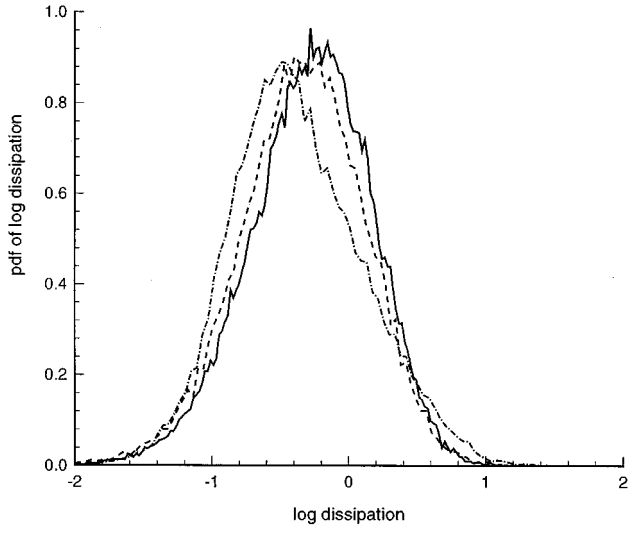

FIG. 7. The pdf of the $\log_{10} \epsilon/\langle\epsilon\rangle$. Solid line—C-$\mathscr{K}_0$[1a], dashed line—C-$\mathscr{K}_0$[1b;0.5], and dot–dashed line—C-$\mathscr{K}_0$[2]. The F-$\mathscr{K}_0$ models exhibit similar behavior.

between the skewness S_3, or dimensionless triple velocity derivative, and $E(k)$, which can be written in the form

$$4\nu^2 \int_{k_c}^{\infty} k^4 E(k)\, dk = -\frac{35}{(15)^{3/2}} S_3 \nu^{-1/2} \epsilon_{\rm sgs}^{3/2}. \tag{48}$$

Experiment indicates a value near $S_3 = -0.5$. Use of (48) in (46) with this value gives closure. It may be objected that this is still a one-parameter model, but unlike the Kolmogorov prefactor, S_3 is a defined (model independent) quantity characteristic of the dissipation range of turbulence which by definition, lies outside the range of resolved scales in LES. Some input from experiment or theory is then justified.

The stretched-vortex ansatz appears able to give a self-consistent if approximate quantitative description of the detailed fine-scale properties of turbulence and at the same time provides a basis for the construction of workable SGS models relating the averaged behavior of the fine scales to the resolved-flow variables in large-eddy simulation. The implementation of a $K-\epsilon_{\rm sgs}$ version of the vortex model, and the application of the present class of vortex SGS models to nonhomogeneous flows including channel and other wall-bounded shear flows, provide topics for future research.

ACKNOWLEDGMENTS

This work was supported in part by NSF Grant CTS-9634222. The authors wish to thank Dr. Thomas Lund for useful discussions and help in the implementation of the decaying test. AM benefited from his visit to CTR during the 1996 Summer Program and would like to thank Professor Parviz Moin for useful suggestions.

APPENDIX: VORTEX EVOLUTION IN A LINEAR RESOLVED FIELD

Consider a vortex embedded in a background linear velocity field, the latter viewed as generated by the velocity gradients of the local resolved flow. Denote laboratory-fixed axes by x_i and vortex-fixed axes by r_i; for clarity we omit the ''prime'' superscipt on vortex-fixed quantities. Without loss of generality these two axis systems may be chosen to be coincident at time $t=0$. The fluid velocity in the fixed frame is q_i and the vorticity is $\xi_i = \varepsilon_{ijk}\partial q_k/\partial x_j$, while in vortex-fixed axes these are v_i and $\zeta_i = \varepsilon_{ijk}\partial v_k/\partial r_j$, respectively, where ε_{ijk} used with a triple subscript here denotes the alternating tensor. The vortex rotates with angular velocity $\Omega_i(t)$ with respect to the x_i in a way to be described. The background field is

$$\tilde{q}_i = \tilde{A}_{ij}(t)x_j \equiv \tilde{S}_{ij}(t)x_j + \tilde{Q}_{ij}(t)x_j, \tag{A1}$$

where $\tilde{S}_{ij}(t)$ is the symmetric and $\tilde{Q}_{ij}(t) = \frac{1}{2}\varepsilon_{ijk}\tilde{\xi}_k(t)$ the antisymmetric part of $\tilde{A}_{ij}(t)$, and $\tilde{\xi}_i(t)$ is the background vorticity. The time dependencies of all these quantities, which differ in laboratory- and in vortex-fixed axes, will be suppressed unless required. In particular we note that the background strain tensor $\tilde{S}_{ij}(t)$ and vorticity $\tilde{\xi}_k(t)$ are not independent, since the latter is subject to stretching and tilting by $\tilde{S}_{ij}(t)$. Let $u_i(\mathbf{r},t)$ be the velocity field associated with the vortex alone, in vortex fixed axes, and ω_i be the correspond-

ing vorticity, $\omega_i=\varepsilon_{ijk}\partial u_k/\partial r_j$. The full velocity and vorticity in the vortex-fixed (rotating) axes are then

$$\zeta_i(\mathbf{r},t)=\tilde{\xi}_i-2\Omega_i+\omega_i, \tag{A2}$$

$$v_i(\mathbf{r},t)=\tilde{A}_{ij}r_j-\varepsilon_{ijk}\Omega_j r_k+u_i. \tag{A3}$$

The components of v_i are

$$\begin{aligned} v_1-u_1&=\tilde{A}_{11}r_1+(\tilde{A}_{12}+\Omega_3)r_2+(\tilde{A}_{13}-\Omega_2)r_3,\\ v_2-u_2&=(\tilde{A}_{21}-\Omega_3)r_1+\tilde{A}_{22}r_2+(\tilde{A}_{23}+\Omega_1)r_3,\\ v_3-u_3&=(\tilde{A}_{31}+\Omega_2)r_1+(\tilde{A}_{32}-\Omega_1)r_3+\tilde{A}_{33}r_3. \end{aligned} \tag{A4}$$

In vortex-fixed axes, the momentum and vorticity equations may be written, respectively, as

$$\frac{\partial}{\partial t}(v_i+\varepsilon_{ijk}\Omega_j r_k)+v_j\frac{\partial v_i}{\partial r_j}+2\varepsilon_{ijk}\Omega_j v_k=\frac{\partial P^*}{\partial r_i}+\nu\nabla^2_{r_i}v_i, \tag{A5}$$

$$\frac{\partial}{\partial t}(\tilde{\zeta}_1+2\tilde{\Omega}_i)+v_j\frac{\partial\tilde{\zeta}_i}{\partial r_j}=(\tilde{\zeta}_j+2\Omega_j)\frac{\partial v_i}{\partial r_j}+\nu\nabla^2_{r_i}\zeta_i, \tag{A6}$$

where $P^*=P+\frac{1}{2}\Omega^2 r_i^2$ and P is the pressure. Continuity is $\partial v_i/\partial r_i=0$.

At $t=0$ we specify that $\omega_i=\omega_i(r_1,r_2,0)$ [hence $u_i=u_i(r_1,r_2,0)$] and $r^2\omega_i\to 0$ as $r_1^2+r_2^2\to\infty$. Thus there is initially no dependence on the r_3 coordinate, which is viewed as the ''axis'' of the vortex, and the vorticity is compact in the cross-sectional plane, (r_1-r_2). It follows from (A4–A6) and the initial conditions that the absence of dependence on r_3, i.e., $\omega_i=\omega_i(r_1,r_2,t)$ and $u_i=u_i(r_1,r_2,t)$, will be preserved in the evolution provided $\Omega_1=-\tilde{A}_{23}$ and $\Omega_2=\tilde{A}_{13}$. The component Ω_3 is arbitrary and a convenient choice is $\Omega_3=-\tilde{A}_{12}$. Introduction of a vector potential $\Psi_i(r_1,r_2,t)$, such that

$$u_i=\varepsilon_{ijk}\frac{\partial\Psi_k}{\partial r_j},\quad \frac{\partial\Psi_i}{\partial r_i}=0,\quad \omega_i=-\nabla^2_{r_i}\Psi_i, \tag{A7}$$

then allows (A4) to be written in the form

$$\begin{aligned} v_1&=\tilde{S}_{11}r_1+\frac{\partial\Psi_3}{\partial r_2},\\ v_2&=2\tilde{S}_{12}r_1+\tilde{S}_{22}r_2-\frac{\partial\Psi_3}{\partial r_1},\\ v_3&=2\tilde{S}_{13}r_1+2\tilde{S}_{23}r_2+\tilde{S}_{33}r_3+\frac{\partial\Psi_2}{\partial r_1}-\frac{\partial\Psi_1}{\partial r_2}. \end{aligned} \tag{A8}$$

When (A8) and (A2) are used in (A6), the resulting equations together with the third of (A7) give closed equations for $\omega_i(r_1,r_2,t)$. Similarly, closed equations for $u_i(r_1,r_2,t)$ may be obtained from (A5).

It is straightforward that the above choice for Ω_i is equivalent to rotation of the r_3 axis according to

$$\frac{\partial e_i}{\partial t}=e_j\tilde{A}_{ij}-e_i e_k e_j\tilde{A}_{kj}, \tag{A9}$$

where $e_i(t)\equiv e_i^v$ (text usage) are the direction cosines of the r_3 axis relative to the laboratory axes $[\mathbf{e}(0)=(0,0,1)]$. This is just the rotation that would be experienced by a material line element of unit length aligned with the vortex axis, due to the linear field alone; it provides a derivation of Eq. (20). The vortex axis remains rectilinear and the internal structure of the vortex is two-dimensional in the sense of dependence only on (r_1,r_2), but allows axial flow.

To obtain the enstrophy equation we simplify to the special case where there is no background vortcity $\tilde{\xi}_i=0$. This may be a reasonable model for a strong vortex $|\omega_i|\gg|\tilde{\xi}_i|$. We also put $\omega_1=\omega_2=0$ at $t=0$, from which it follows from the vorticity equation that this will be true for all $t>0$. The ω_3 vorticity equation is then

$$\frac{\partial\omega_3}{\partial t}+\left(\tilde{S}_{11}r_1+\frac{\partial\Psi_3}{\partial r_2}\right)\frac{\partial\omega_3}{\partial r_1}+\left(2\tilde{S}_{12}r_1+\tilde{S}_{22}r_2-\frac{\partial\Psi_3}{\partial r_1}\right)\frac{\partial\omega_3}{\partial r_2}=\tilde{S}_{33}\omega_3+\nu\nabla^2_{r_i}\omega_3. \tag{A10}$$

Now multiply (A10) by ω_3, integrate over the (r_1-r_2) plane, and use the well-known results, valid for the vortex flow, $\overline{\nu\omega_3\nabla^2_{r_i}\omega_3}=2\nu\int_0^\infty k^4E(k)dk$ and $\epsilon_{\rm sgs}=\overline{\nu\omega_3^2}$, where $E(k)$ is the shell-summed energy spectrum and where the overbar refers to an integral over the vortex cross section. This gives, after some algebra,

$$\frac{\partial\overline{\epsilon_{\rm sgs}}}{\partial t}=\tilde{S}_{33}\overline{\epsilon_{\rm sgs}}-4\nu^2\int_0^\infty k^4E(k)\,dk. \tag{A11}$$

Finally, we account for the stretching or compression of the vortex by $\tilde{S}_{33}$ and for an average over all possible spin angles of the vortex structure about the r_3 axis. Denoting the vortex length at time by $l(t)$, we write for some quantity f

$$\begin{aligned} \bar{\bar{f}}&=\frac{l(t)}{2\pi L^3}\int_{-\infty}^{\infty}\int_{-\infty}^{\infty}\int_0^{2\pi}f\,dr_1dr_2d\gamma,\\ l(t)&=l(0)\exp\left(\int_0^t\tilde{S}_{33}(t')dt'\right), \end{aligned} \tag{A12}$$

where the double overbar denotes integration over r_3 [equivalent to multiplying by $l(t)$] and the vortex cross section, division by the volume L^3 of a large box containing a vortex and an average over all possible spin angles γ, $0\leqslant\gamma\leqslant 2\pi$. Differentiating the first of (A12) with respect to t and using the second of (A12) then gives

$$\frac{\partial\bar{\bar{f}}}{\partial t}=\tilde{S}_{33}\bar{\bar{f}}+\frac{\partial}{\partial t}\left(\frac{l(t)}{2\pi L^3}\int_{-\infty}^{\infty}\int_{-\infty}^{\infty}\int_0^{2\pi}f\,dr_1dr_2d\gamma\right). \tag{A13}$$

When the first of (A12) is applied to (A11) ($f\equiv\epsilon_{\rm sgs}$) and (A13) is used for the unsteady term it is found that

$$\frac{\partial\bar{\bar{\epsilon}}_{\rm sgs}}{\partial t}=2\tilde{S}_{33}\bar{\bar{\epsilon}}_{\rm sgs}-4\nu^2\int_0^\infty k^4E(k)\,dk, \tag{A14}$$

and we note that the double overbar has been suppressed for $E(k)$. Omitting the double overbar on the other terms gives Eq. (46).

An energy equation for the internal vortex motions may be obtained along similar lines, starting with (A5). Care must be taken to account for the contribution from the pressure at infinity in the r_1-r_2 plane and the time variation of $\tilde{S}_{ij}(t)$ in

the vortex-fixed frame. Defining $K=\frac{1}{2}(\overline{\overline{u_1^2}}+\overline{\overline{u}_2})$ and invoking equipartition $\overline{\overline{u_1^2}}=\overline{\overline{u_2^2}}$, $\overline{\overline{u_1 u_2}}=0$ in vortex-fixed axes following averaging over spin angle, and using

$$\frac{l(t)}{2\pi L^3}\int_0^{2\pi}\nu\overline{\overline{(u_1\nabla_{r_i}^2 u_1+u_2\nabla_{r_i}^2 u_2)}}\,d\gamma$$

$$=-2\nu\int_0^\infty k^2E(k)\,dk, \tag{A15}$$

one obtains, after some algebra,

$$\frac{\partial K}{\partial t}=\tilde{S}_{33}K-2\nu\int_0^\infty k^2E(k)\,dk. \tag{A16}$$

[1] A. Leonard, ''Energy cascade in large-eddy simulations of turbulent fluid flows,'' *Advances in Geophysics*, edited by F. N. Frankiel and R. E. Munn (Academic, New York, 1974), Vol. 18A, pp. 237–248.

[2] R. S. Rogallo and P. Moin, ''Numerical simulation of turbulent flows,'' Annu. Rev. Fluid Mech. **16**, 99 (1984).

[3] J. Smagorinsky, ''General circulation experiments with primitive equations,'' Mon. Weather Rev. **91**, 99 (1963).

[4] M. Germano, U. Piomelli, P. Moin, and W. H. Cabott, ''A dynamic subgrid scale eddy-viscosity model,'' Phys. Fluids A **3**, 1760 (1991).

[5] S. Ghosal, T. S. Lund, P. Moin, and K. Akselvoll, ''A dynamic localization model for large-eddy simulation of turbulent flows,'' J. Fluid Mech. **286**, 229 (1995).

[6] W. C. Reynolds, ''The potential and limitations of direct and large eddy simulations,'' in *Whither Turbulence? Turbulence at the Crossroads*, edited by J. L. Lumley (Springer Verlag, New York, 1989), p. 313.

[7] M. Lesieur and O. Metais, ''New trends in large-eddy simulation,'' Annu. Rev. Fluid Mech. **28**, 45 (1996).

[8] W. C. Reynolds, ''Towards a structure-based turbulence model,'' in *Studies in Turbulence*, edited by T. B. Gatski *et al.* (Springer Verlag, New York, 1992), p. 76.

[9] D. I. Pullin, and P. G. Saffman, ''Reynolds stresses and one-dimensional spectra for a vortex model of homogeneous anisotropic turbulence,'' Phys. Fluids **6**, 1787 (1994).

[10] W. C. Reynolds and S. Kassinos, ''One-point modeling of rapidly deformed homogeneous turbulence,'' Proc. R. Soc. London Ser. A **451**, 87 (1995).

[11] W. T. Ashurst, A. R. Kerstein, R. M. Kerr, and C. H. Gibson, ''Alignment of vorticity and scalar-gradient in simulated Navier-Stokes turbulence,'' Phys. Fluids **30**, 2343 (1987).

[12] A. Vincent and M. Meneguzzi, ''The spatial structure and statistical properties of homogeneous turbulence,'' J. Fluid Mech. **225**, 1 (1991).

[13] A. A. Townsend, ''On the fine-scale structure of turbulence,'' Proc. R. Soc. London Ser. A **208**, 534 (1951).

[14] T. S. Lundgren, ''Strained spiral vortex model for turbulent fine structure,'' Phys. Fluids **25**, 2193 (1982).

[15] D. I. Pullin and P. G. Saffman, ''On the Lundgren–Townsend model of turbulent fine scales,'' Phys. Fluids A **5**, 126 (1993).

[16] D. I. Pullin, J. D. Buntine, and P. G. Saffman, ''On the spectrum of a stretched spiral vortex,'' Phys. Fluids **6**, 3010 (1994).

[17] W. J. Cocke, ''Turbulent hydrodynamic line stretching—Consequences of isotropy,'' Phys. Fluids **12**, 2488 (1969).

[18] S. A. Orszag, ''Comments on: Turbulent hydrodynamic line stretching—Consequences of isotropy,'' Phys. Fluids **13**, 2203 (1970).

[19] S. Kida and Y. Murakami, ''Kolmogorov similarity in freely decaying turbulence,'' Phys. Fluids **30**, 2030 (1987).

[20] S. G. Saddoughi and S. V. Veeravalli, ''Local isotropy in turbulent boundary layers at high Reynolds number,'' J. Fluid Mech. **268**, 333 (1994).

[21] G. Comte-Bellot and S. Corrsin, ''Simple Eulerian time correlation of full and narrow-band velocity signals in grid-generated 'isotropic' turbulence,'' J. Fluid Mech. **48**, 273 (1971).

[22] D. Carati, S. Ghosal, and P. Moin, ''On the representation of backscatter in dynamic localization models,'' Phys. Fluids **7**, 606 (1995).

[23] R. M. Kerr, ''Higher-order derivative correlations and the alignment of small-scale structures in isotropic numerical turbulence,'' J. Fluid Mech. **153**, 31 (1985). See also NASA TM (84407) (1983).

[24] P. Mason and D. Thomson, ''Stochastic backscatter in large-eddy simulation of boundary layers,'' J. Fluid Mech. **242**, 51 (1992).